

Contents lists available at ScienceDirect

#### Petroleum Science

journal homepage: www.keaipublishing.com/en/journals/petroleum-science



#### Original Paper

# Study of steam heat transfer enhanced by CO<sub>2</sub> and chemical agents: In heavy oil production



Ya-Li Liu a, b, Chao Zhang a, b, Song-Yan Li a, b, Zhao-Min Li a, b, \*

- <sup>a</sup> Key Laboratory of Unconventional Oil & Gas Development (China University of Petroleum (East China)), Ministry of Education, Qingdao, 266580, Shandong, PR China
- <sup>b</sup> School of Petroleum Engineering, China University of Petroleum (East China), Qingdao, 266580, Shandong, PR China

#### ARTICLE INFO

Article history:
Received 1 April 2022
Received in revised form
27 September 2022
Accepted 28 September 2022
Available online 4 October 2022

Edited by Yan-Hua Sun

Keywords:
Steam flooding
Heavy oil
Carbon dioxide
Chemical agent
Enhanced oil recovery (EOR)
Heat transfer

#### ABSTRACT

Steam flooding with the assistance of carbon dioxide  $(CO_2)$  and chemicals is an effective approach for enhancing super heavy oil recovery. However, the promotion and application of  $CO_2$  and chemical agent-assisted steam flooding technology have been restricted by the current lack of research on the synergistic effect of  $CO_2$  and chemical agents on enhanced steam flooding heat transfer. The novel experiments on  $CO_2$ —chemicals cooperate affected steam condensation and seepage were conducted by adding  $CO_2$  and two chemicals (sodium dodecyl sulfate (SDS) and the betaine temperature-salt resistant foaming agent ZK-05200).

According to the experimental findings, a "film" formed on the heat-transfer medium surface following the co-injection of  $CO_2$  and the chemical to impede the steam heat transfer, reducing the heat transfer efficiency of steam, heat flux and condensation heat transfer coefficient. The steam seepage experiment revealed that the temperature at the back end of the sandpack model was dramatically raised by 3.5-12.8~ °C by adding  $CO_2$  and chemical agents, achieving the goal of driving deep-formation heavy oil. The combined effect of  $CO_2$  and SDS was the most effective for improving steam heat transfer, the steam heat loss was reduced by 6.2%, the steam condensation cycle was prolonged by 1.3 times, the condensation heat transfer coefficient was decreased by 15.5%, and the heavy oil recovery was enhanced by 9.82%. Theoretical recommendations are offered in this study for improving the  $CO_2$ -chemical-assisted steam flooding technique.

© 2023 The Authors. Publishing services by Elsevier B.V. on behalf of KeAi Communications Co. Ltd. This is an open access article under the CC BY-NC-ND license (http://creativecommons.org/licenses/by-nc-nd/4.0/).

#### 1. Introduction

With drastic increase in the global demand for crude oil in recent years, heavy oil resources have had an increasingly important role in fossil energy sources (Guo et al., 2016). The most common approaches for heavy oil development mainly include thermal methods (i.e., with heat injection, such as cyclic steam stimulation, steam-assisted gravity drainage, and *in-situ* combustion) (Li, 2012; Shi et al., 2010; Li et al., 2017) and cold production technology (i.e., without heat injection, such as water flooding, water-alternating gas, cyclic solvent injection, and vapour extraction) (Ma et al., 2020; Tian et al., 2022; Aklilu et al., 2018). Previous

E-mail address: lizhm@upc.edu.cn (Z.-M. Li).

studies have reported that steam flooding is one of the most effective methods for enhancing heavy oil recovery. It is suitable for the development of reservoir with a viscosity in the range of 10000–50000 mPa·s, thick oil layer, no edge, and bottom water reservoirs (Alvarado and Manrique, 2010). However, issues such as steam overlay and gas channeling exist in the late stage of steam flooding, making it impossible for steam flooding to overcome heat transport in superheavy oil reservoirs (Li et al., 2022a). New theories and technologies were proposed to address the aforementioned issues, such as CO<sub>2</sub>—chemical cooperative-assisted steam flooding technology.

Steam heating, gas increasing reservoir energy, oil swelling, interfacial tension decrease, hydrocarbon extraction, and chemical emulsification to reduce oil viscosity are the main mechanisms of CO<sub>2</sub>—chemical, cooperative assisted steam flooding to enhance heavy oil recovery (Wan et al., 2020; Ahmadi and Chen, 2020). Moreover, CO<sub>2</sub>—chemical assisted steam technology successfully

<sup>\*</sup> Corresponding author. Key Laboratory of Unconventional Oil & Gas Development (China University of Petroleum (East China)), Ministry of Education, Qingdao, 266580, Shandong, PR China.

absorbed and sequestered CO<sub>2</sub>, contributing to reducing greenhouse gas emissions (Wang et al., 2022; Wu et al., 2018).

In recent years, research on CO2-chemical assisted steam flooding technology has been conducted. Pang et al. designed a horizontal well model, and Liu et al. developed a thin heavy oil reservoir model, both of which investigated the effects of CO2 injection on the steam drive mechanism (Pang et al., 2018; Liu et al., 2017). However, CO<sub>2</sub> channeling was observed in the early stages of the experiment. To address the issue of gas channeling, Hou et al. employed polymer gel to inhibit CO<sub>2</sub> channeling (Hou et al., 2017). In the Sunset oil field in the United States, Mukherjee et al. used a low-cost surfactant solution to effectively prevent steam channeling and overlapping (Mukherjee et al., 2018). Li et al. assisted steam flooding by using CO<sub>2</sub> and surfactant. In the experimental model, the multiphase foam developed and effectively prevented CO<sub>2</sub> channeling. In addition, the emulsion of surfactant and CO<sub>2</sub> may reduce the viscosity of heavy oil by 95%, increasing heavy oil recovery by 13% (Li et al., 2022b). According to Wang et al.'s research, temperature, mass fraction of chemical agents, and their interaction were the primary mechanisms for enhancing oil recovery. These factors accounted for 92.7% of the weight in improving oil recovery (Wang et al., 2017). Zare and Hamouda (2019) carried out an experimental evaluation of the impact of carbon atoms (C<sub>6</sub> and C<sub>7</sub>) on steam flooding. The results showed that the formation energy augmentation and oil viscosity decrease attributed to CO<sub>2</sub> expansion were the major factors behind the increase in heavy oil fluidity (Zare and Hamouda, 2019).

The expansion of the steam chamber and the alteration of the temperature field are the fundamental components of steam flooding technology. Canbola et al. observed that the insulating effect of the gas accumulated at the top of the reservoir controlled the heat loss in the steam chamber (Canbolat et al., 2013). Law pointed out that the noncondensate gas input into the steam chamber served a variety of purposes, including the formation of energy, preserving formation pressure, reducing vapour partial pressure, and stabilizing the steam chamber (Law, 2004). The Dover project in Canada demonstrated that expanding noncondensate gas and surfactants may significantly decrease the depletion of the steam chamber, leading to better recovery of heavy oil (Sharma and Gates, 2010).

Notably, prior work on CO<sub>2</sub>—chemical assisted steam technology primarily focused on enhancing heavy oil recovery and disregarded reservoir heat transfer research. In oil and gas development engineering, the heavy oil viscosity significantly decreased when the temperature increased. The temperature change was dependent on steam condensation heat transfer and had a substantial influence on improving heavy oil recovery (Xu et al., 2020). Previously, our research group demonstrated the influence of noncondensate gas on steam condensation heat transfer, and pertinent scientific articles have been published (Wang et al., 2019, 2020).

However, there is a lack of mechanistic research on how CO<sub>2</sub> and chemicals cooperate enhance steam heat transfer, including how to alter the method of steam condensation, how to encourage the growth of steam chambers, and how to influence the movement of steam fronts in porous media (Dong et al., 2021). To improve the heat transfer of steam flooding in the reservoir, the mechanism of the CO<sub>2</sub>—chemical combination must be refined.

Therefore, in this study, steam heat transfer and seepage experiments were conducted to evaluate ternary composite-enhanced thermal oil recovery technology. Based on the steam condensation modes and the observed heat transfer coefficient, the optimized steam heat transfer characteristics were obtained. From the standpoint of steam—CO2—chemical interactions and their impact on steam condensation heat transfer, the influencing parameters, such as the steam injection rate, gas injection rate,

undercooling degree, and chemical agent content were explored.

#### 2. Experimental

#### 2.1. Materials

The steam was produced by a GL-1 steam generator. Ultrapure water was produced by a UPT-I-10T water purifier (Sichuan Youpu Ultrapure Technology Co., Ltd.). The carbon dioxide was provided by Qingdao Tianyuan Gas Manufacturing (China), with a purity of 99.9 mol%. Sodium dodecyl sulfate (SDS) with a purity of >99.0% was supplied by Sigma (USA). The temperature and salt-resistant foaming agent (ZK-05200) with a purity of >99.0% was supplied by Qingtian Zhongke Plant Technology Co., Ltd. (China). The crude oil was collected from Shengli Oilfield, China, with a viscosity of 238.7 mPa·s and a density of 920 kg/m³ at 65 °C.

#### 2.2. Apparatus

#### 2.2.1. Steam condensation experiments

The steam condensation experiment apparatus used in this study is shown in Fig. 1a. The GL-1 steam generator was provided by the Hai'an Petroleum Scientific Research Instrument Company. The maximum output temperature of the steam was 250  $^{\circ}$ C, and the maximum pressure was 25 MPa. The high-precision plunger pump (100DX model, Teledyne ISCO, USA) has a maximum output pressure of 66 MPa, a maximum output flow of 60 mL/min, and an accuracy of 0.001 mL/min. A heating band was used to insulate the pipeline between the steam generator and the condensate chamber to reduce heat loss during steam injection. The gas flow controller (Brooks SLA5850S) has a flow range of 0–50 mL/min and an accuracy of 0.1 mL/min. The controlled gas flow exhibited long-term zero stability, with an annual variation of less than  $\pm 0.5\%$  of the full scale.

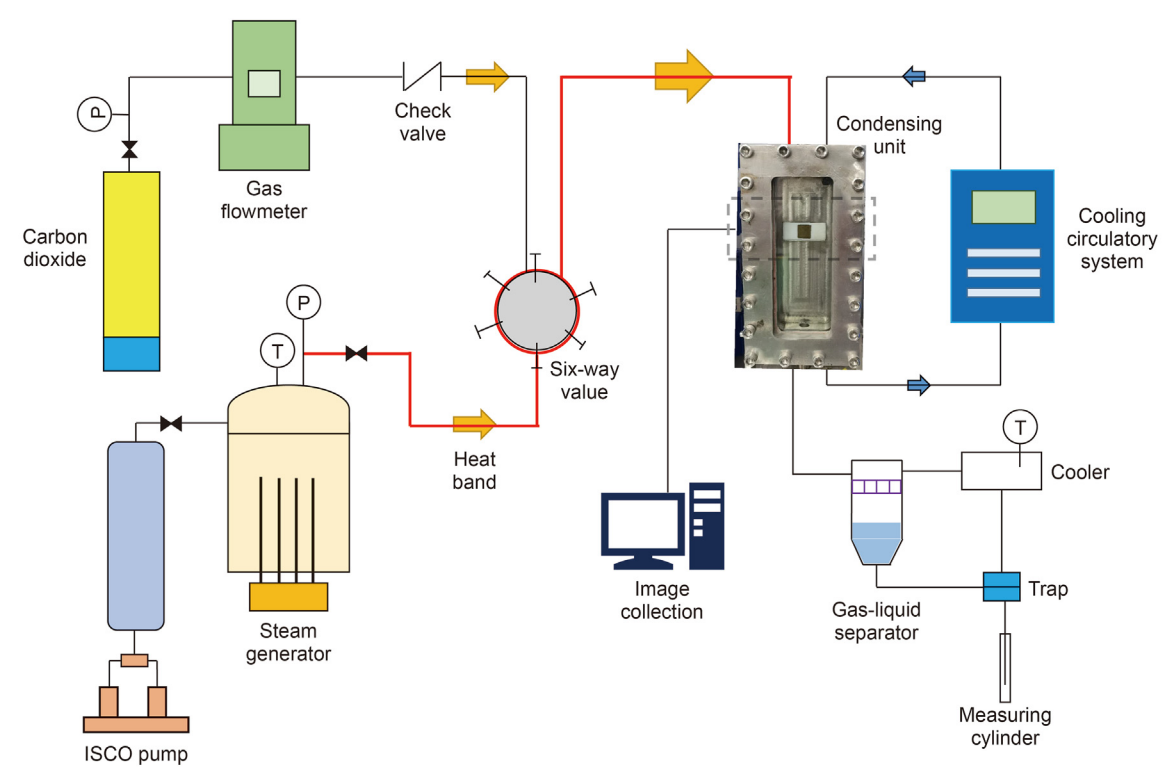
The condensation unit employed in the experiment was constructed of stainless steel, which could endure a temperature of 280 °C and a pressure of 5 MPa. The size of the condensation chamber was 140 mm  $\times$  20 mm  $\times$  300 mm. The condensate condensation was equipped with a brass-based condensing block, as shown in Fig. 1b.

To ensure that the surface was smooth, the condensation surface was polished with sandpaper and then soaked in a mixture of pure alcohol and 20% sulfuric acid. The brass-based condensing block and stainless steel contact parts were insulated by polytetra-fluoroethylene (PTFE). Five K-type thermocouples with a diameter of 0.4 mm and a measuring accuracy of 0.01 °C were installed in the detection holes. The detection holes were evenly distributed in the brass-based condensing block. The K-type thermocouples were distributed with a spacing of 2 mm and a penetration depth of 10 mm. The standard error was less than 10%.

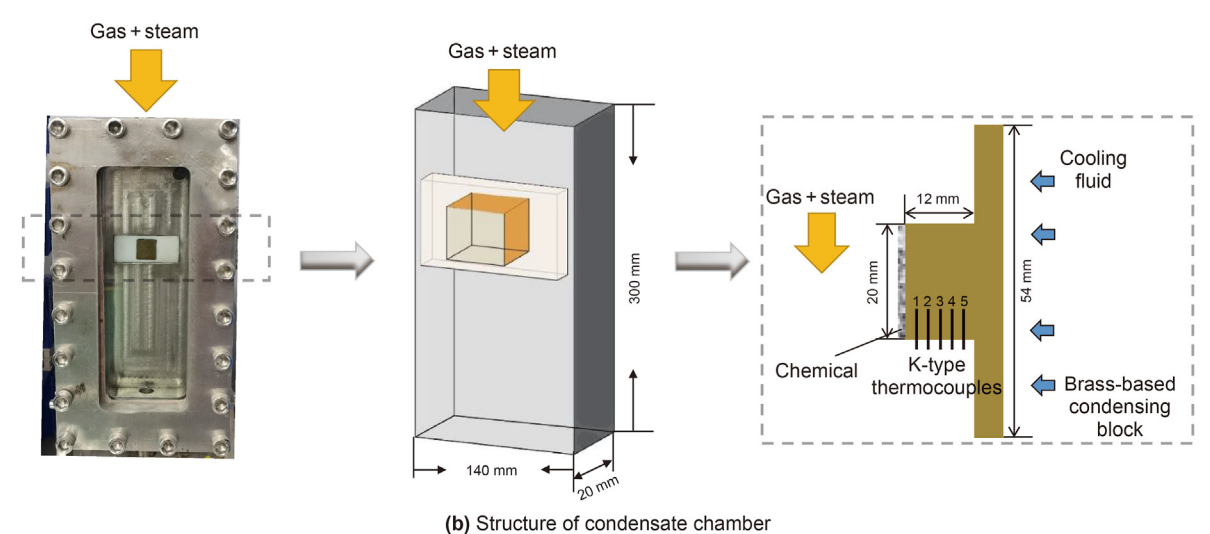
#### 2.2.2. Steam seepage experiment

The experimental apparatus had the same steam generator, pump, and gas flow controller as those mentioned in Section 2.2.1 and shown in Fig. 2a. The back pressure value and one-dimensional sandpack model were produced by the Hai'an Petroleum Scientific Research Instrument Company. The accuracy of the back pressure value was 0.1 MPa. The sandpack model was 2.5 cm in diameter and 60 cm in length; the size of silica sand used to make the sandpack model was 120 and 70 mesh; and three temperature measuring points were placed 5, 30, and 55 cm from the sandpack model entrance. The balance (MS 2045) was provided by METTLER TOLEDO Company, with a range of 0–1000 g and an accuracy of 0.01 g.

To reduce heat dissipation, the inner wall of the sandpack was equipped with a resin thermal-insulating layer, as shown in Fig. 2b.



(a) Experimental equipment for steam condensation



(b) Structure of condensate chamber

Fig. 1. Schematic of steam condensation experiment.

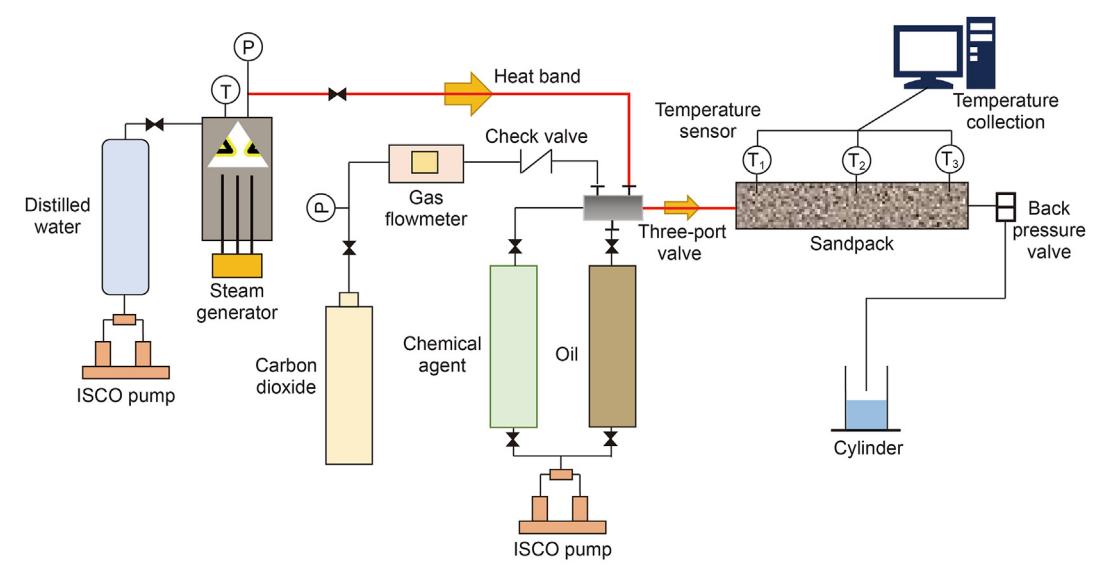
### 2.3.1. Steam condensation

2.3. Experimental procedures

- (1) The gas tightness of the condensing chamber was gauged by a pressurization method. After connecting the equipment, the cooling circulation system and steam generator were started. The surface of brass-based condensing block was used to simulate the low-temperature porous media in the reservoirs.
- (2) Steam was injected from the top entrance of the condensing chamber after the temperature stabilized. Next, the condensation behaviour on the surface of the brass-based condensing block was examined, the condensate water was
- collected, and the temperature of the K-type thermocouples was recorded in real-time until the condensation heat transfer stabilized. Condensation heat transfer stability was defined as the state in which the surface temperature of the brass-based condensing block was constant.
- (3) The steam injection temperature was 250 °C, the steam injection rate was modified to 5, 10, and 20 mL/min; and the undercooling was altered to 20, 40, and 60 °C. Step (2) was repeated to conduct the heat transfer experiment with various influencing factors.

#### 2.3.2. CO<sub>2</sub>—chemical assisted steam condensation

The preparation step procedures matched those used in the



(a) Experimental equipment for steam seepage experiment



(b) 1D sandpack with temperature measuring function and thermal-insulating layer

Fig. 2. Schematic of steam seepage experiment in 1D sandpack model.

steam condensation experiment. The condensing block surface was coated with 0.05 PV chemical agents at room temperature. The steam injection temperature was kept at 250 °C, the injection rate was 5 mL/min, and the degree of undercooling was set at 20 °C. The CO $_2$  injection speed was changed to 5, 10, and 20 mL/min to investigate the mechanism of adding CO $_2$  and chemical agents during steam condensation heat transfer.

#### 2.3.3. Steam-CO<sub>2</sub>-chemical seepage

- (1) A sandpack model with a permeability of 800–830 mD and a porosity of 32%–34% was prepared, and the gas tightness of the sandpack model was checked. The sandpack model was then vacuumed and saturated with oil.
- (2) The prepared sandpack model was placed in a 65 °C thermostat. In the CO<sub>2</sub>—chemical assisted steam seepage experiment, steam and CO<sub>2</sub> coinjection were performed. When the water saturation of the produced fluid reached 98%, a 0.1 PV chemical slug was injected at room temperature. The injection of steam and CO<sub>2</sub> continues.
- (3) The steam temperature was set to 250 °C, and the concentration of chemical agents was 0.5 wt%. The steam injection rate was changed to 0.5, 1, 1.5, 3, and 5 mL/min. The experimental pressure was varied to 1, 2, 3, 4, and 5 MPa.

(4) During the CO<sub>2</sub>—chemical assisted steam seepage experiment, temperature changes at three measurement points on the sandpack model were monitored and recorded in real time. The experiment was halted when the temperature of the sandpack model stabilized.

#### 3. Experimental results and discussion

#### 3.1. Data processing and uncertainty analysis

The temperature was measured on the cooling surface and steam condensation surface. The steam condensation surface temperature  $T_{\rm S}$  was measured by five K-type thermocouples, and the cooling surface temperature  $T_{\rm C}$  was provided by the condensing cycle system. In this paper, the condensation heat transfer coefficient calculation was improved through the thermal equilibrium method.

The following assumptions were made:

(1) The length, width and thickness of the brass-based condensing block were 54, 20, and 12 cm, respectively, indicating that the length and width were significantly larger than the thickness. The sides of the condensing block were insulated with PTFE. Consequently, the heat loss from the

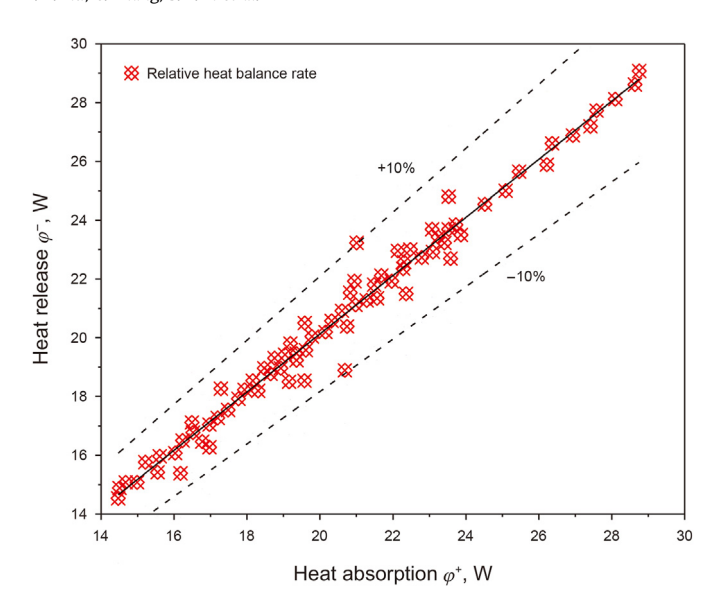


Fig. 3. Error analysis of relative heat balance rate.

sides of the condensing block was ignored (Azad and Trivedi, 2019).

- (2) During the late stage of each experiment, the temperature at each thermocouple tended to remain steady with minimal temperature variation. Condensation heat transfer was assumed to reach a steady state, and the influence of minute temperature variations on heat transfer was ignored.
- (3) The brass-based condensing block was regarded as an infinite monolayer flat wall, and the heat conduction of the condensing block was regarded as one-dimensional constant heat conduction parallel to the cooling surface and the surface through which the steam flowed (Balaji et al., 2021).
- (4) Since a sufficiently long condensation conduit was connected to the condensation chamber, it was assumed that the injected steam had entirely condensed and was released as condensate water.

The condensation heat transfer coefficient was calculated as follows:

(1) Heat absorption on the cooling surface:

$$\varphi^{+} = q_{cf}c_{w}\left(T_{cf,out} - T_{cf,in}\right) \tag{1}$$

where  $\varphi^+$  is the heat flow on the cooling surface, W;  $q_{cf}$  is the mass flow of the cooling fluid, kg/h;  $c_{w}$  is the specific heat capacity of the cooling circulating fluid (specific heat capacity of water), J/(kg·K);  $T_{cf,in}$  and  $T_{cf,out}$  are the injection temperature and circulating discharge temperature of the cooling circulating fluid, respectively, K.

(2) Average convective heat transfer coefficient on the cooling surface (Brame et al., 2019):

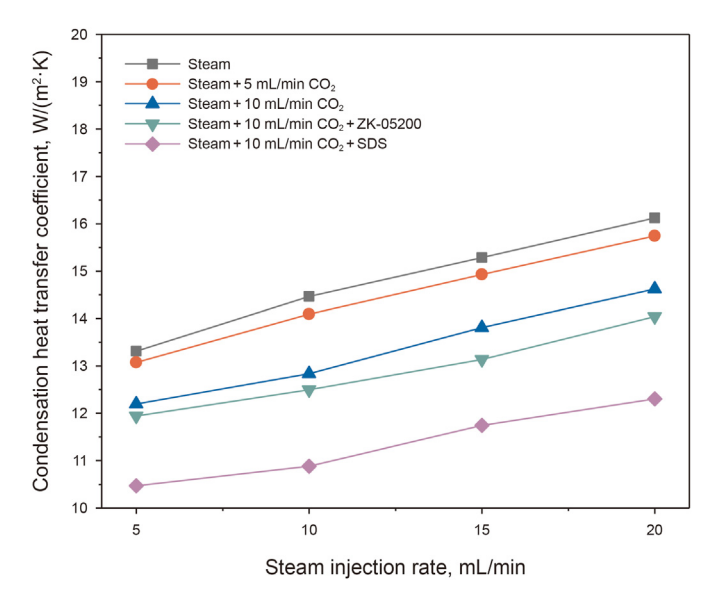


Fig. 4. Influence of injection methods on condensation heat transfer coefficient.

$$h_{\rm cf} = \varphi^+ / A_{\rm cf} \left( \overline{T_{\rm c}} - \overline{T_{\rm cf}} \right) \tag{2}$$

where  $h_{cf}$  is the convective heat transfer coefficient on the cooling surface, W/( $m^2$ ·K);  $A_{cf}$  is the cooling surface area of the condensate block,  $m^2$ ; and  $\overline{T_c}$  is the average temperature of the cooling circulation surface, K.

(3) Heat release on the steam condensation surface:

$$\varphi^{-} = q_{s}c_{s}(T_{s,in} - T_{s}) + q_{co_{2}}c_{co_{2}}(T_{co_{2},out} - T_{co_{2},in})$$
(3)

where  $q_s$  and  $q_{co_2}$  are the heat flow of steam and  $CO_2$ , respectively, kg/h;  $T_{s,in}$  is the injection temperature of steam, K;  $T_s$  is the temperature on the steam condensation surface, K;  $c_{co_2}$  is the specific heat capacity of  $CO_2$ , J/(kg·K);  $T_{co_2,out}$  and  $T_{co_2,in}$  are the injection temperature and discharge temperature, respectively, of  $CO_2$ , K.

(4) Average heat flow:

$$\varphi = \left(\varphi^- + \varphi^+\right) / 2 \tag{4}$$

(5) Relative heat balance rate:

$$\alpha = (\varphi^- - \varphi^+) / \varphi \times 100\% \tag{5}$$

(6) Logarithmic mean temperature difference:

$$\Delta T = \left(T_{\text{cf,out}} - T_{\text{cf,in}}\right) / \ln\left[\left(T_{\text{s}} - T_{\text{cf,in}}\right) / \left(T_{\text{s}} - T_{\text{cf,out}}\right)\right]$$
 (6)

where  $\Delta T$  is the logarithmic mean temperature difference, K.

(7) Overall heat transfer coefficient:

 Table 1

 Effects of different injection systems on heat flux.

Injection method	Steam	$Steam + CO_2$	$Steam + CO_2 + ZK\text{-}05200$	$Steam + CO_2 + SDS$
Heat flux, W/m <sup>2</sup>	188.29	183.92	164.01	143.68

 Table 2

 Experimental parameters of condensation and heat transfer.

No.	Injection method	Steam injection rate, mL/min	Undercooling degree, °C	CO <sub>2</sub> injection rate, mL/min	Type of chemical agent
1	Steam	5	20	_	_
2	Steam	10	20	_	_
3	Steam	20	20	_	_
4	Steam	10	40	_	_
5	Steam	10	60	_	_
6	$Steam + CO_2 + chemical$	5	20	5	SDS
7	$Steam + CO_2 + chemical$	5	20	10	SDS
8	$Steam + CO_2 + chemical$	5	20	20	SDS
9	$Steam + CO_2 + chemical \\$	5	20	10	Foaming agent (ZK-05200)

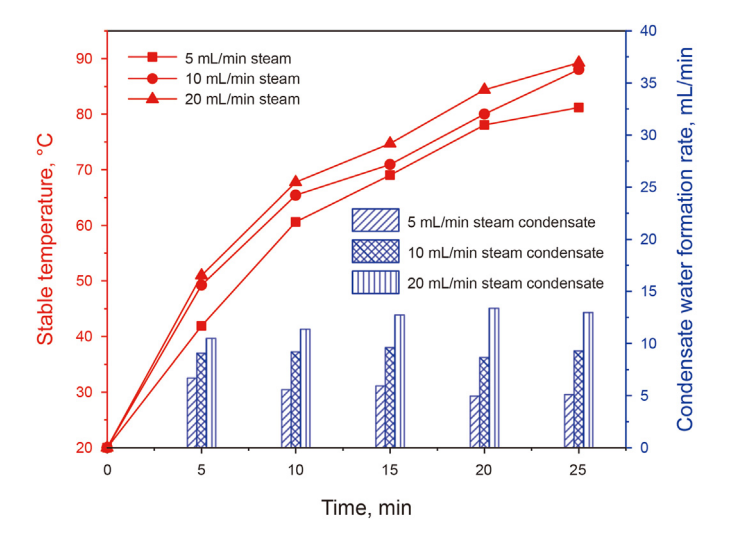
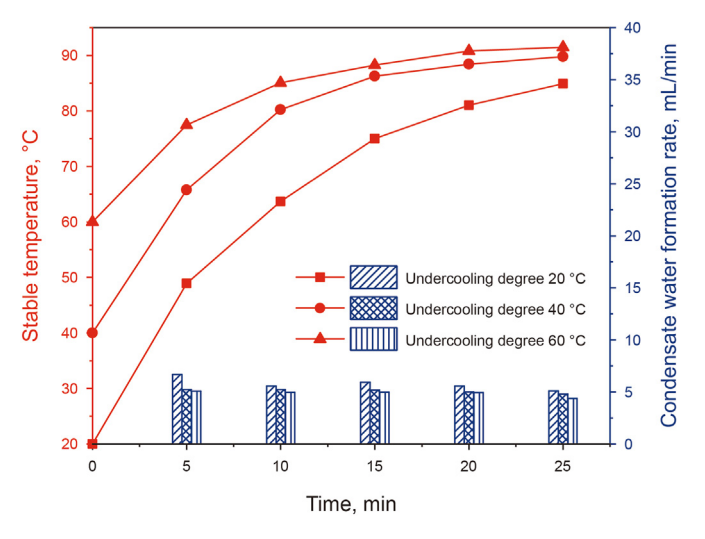


Fig. 5. Effects of steam injection rate on stable temperature and condensate water rate.



**Fig. 6.** Temperature and condensate water rate under the influence of the degree of undercooling.

$$h = \varphi / A_{\rm cf} \Delta T \tag{7}$$

where *h* is the overall heat transfer coefficient,  $W/(m^2 \cdot K)$ .

(8) Heat transfer coefficient on the steam injection surface:

The steam condensation surface temperature was measured by

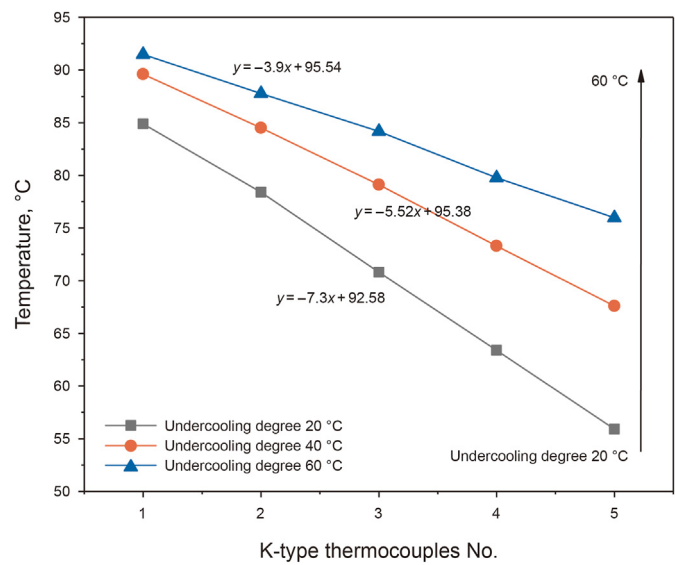


**Fig. 7.** Stable temperature of the K-type thermocouples versus the degree of undercooling.

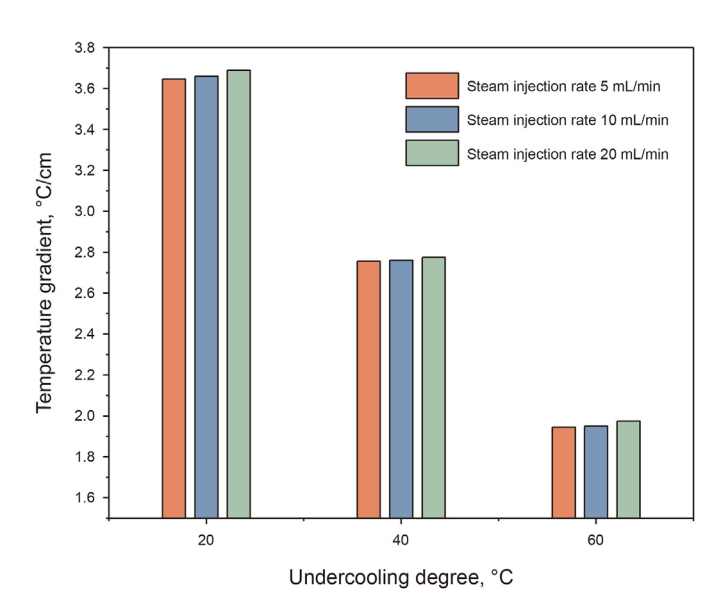


**Fig. 8.** Temperature gradient varies with the steam injection rate and the degree of undercooling.

K-type thermocouples. However, the thermocouples installed in the groove cannot completely cease contact with the condensate block. Therefore, the contact thermal resistance (*R*) between the

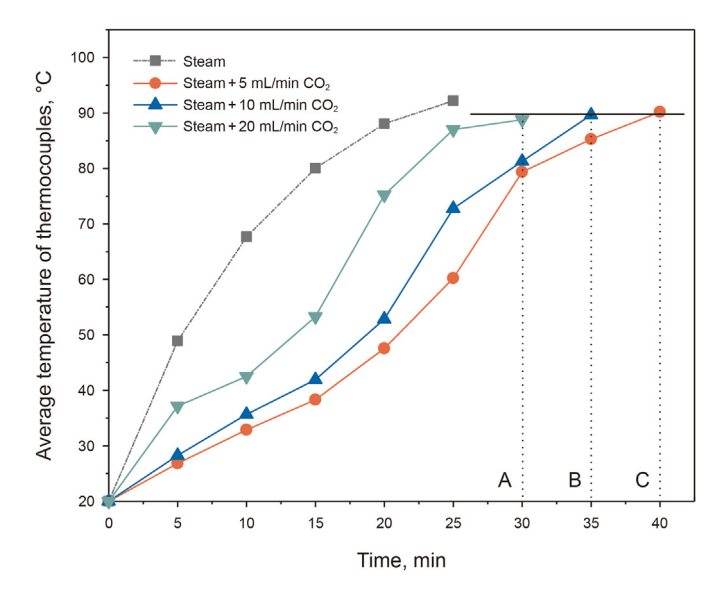


Fig. 9. Change of stable temperature affected by CO2 injection rate.

thermocouples and the condensate block should be considered. The contact thermal resistance was assumed to be a constant value in the experiments.

Knowing the average convective heat transfer coefficient on the cooling surface ( $h_{cf}$ ) and the contact thermal resistance (R), the heat transfer coefficient on the steam injection surface ( $h_i$ ) is obtained according to the following formula (Hasan et al., 2005):

$$1/h=1/h_{cf}+A_{cf}/(h_sA_s)$$
 (8)

where  $h_s$  is the steam condensation heat transfer coefficient, W/ (m<sup>2</sup>·K); and  $A_s$  is the steam condensation surface area of the condensate block, m<sup>2</sup>.

In the steam condensation experiment, the heat flow of steam injection was 300–1200 kg/h. The experimental pressure was 0.1 MPa, and the heat flow of cooling water in the cooling circulation system was 3000–5000 kg/h. Fig. 3 shows the relative heat balance rate of the cooling fluid and steam for different experimental settings.

The relative heat balance rate data greater than 99% was within

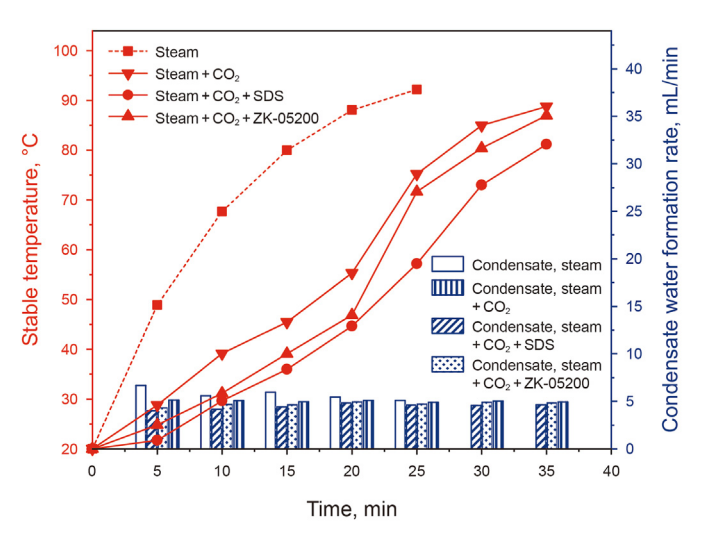


Fig. 11. Influence of steam—CO<sub>2</sub>—chemical on temperature and condensate water rate.

±10%, indicating that the experimental results were reasonable. For the steam condensation and CO<sub>2</sub>—chemical assisted steam condensation experiments, the heat flux and condensation heat transfer coefficient were computed, as shown in Table 1 and Fig. 4.

Fig. 4 indicates that when the CO<sub>2</sub> injection rate was increased, the CO<sub>2</sub> concentration on the condensation surface increased, and the partial steam pressure decreased. The steam saturation temperature and the driving temperature difference in heat transfer decreased, preventing steam heat transfer, and decreasing the condensation heat transfer coefficient. The added chemical was adsorbed on the condensation surface to form a thermal resistance layer, reducing the condensation heat transfer coefficient.

The coefficient was decreased by 15.90% with  $CO_2$ –SDS injection and decreased by 3.99% with  $CO_2$ –ZK-05200 injection. Therefore, the  $CO_2$  and SDS cooperative injection was optimal for reducing the heat transfer between the steam and the condensation media.

#### 3.2. Condensation and heat transfer enhanced by CO<sub>2</sub>—chemicals

The experimental parameters for the steam and  $CO_2$ —chemical assisted steam condensation and heat transfer experiments are summerized in Table 2.

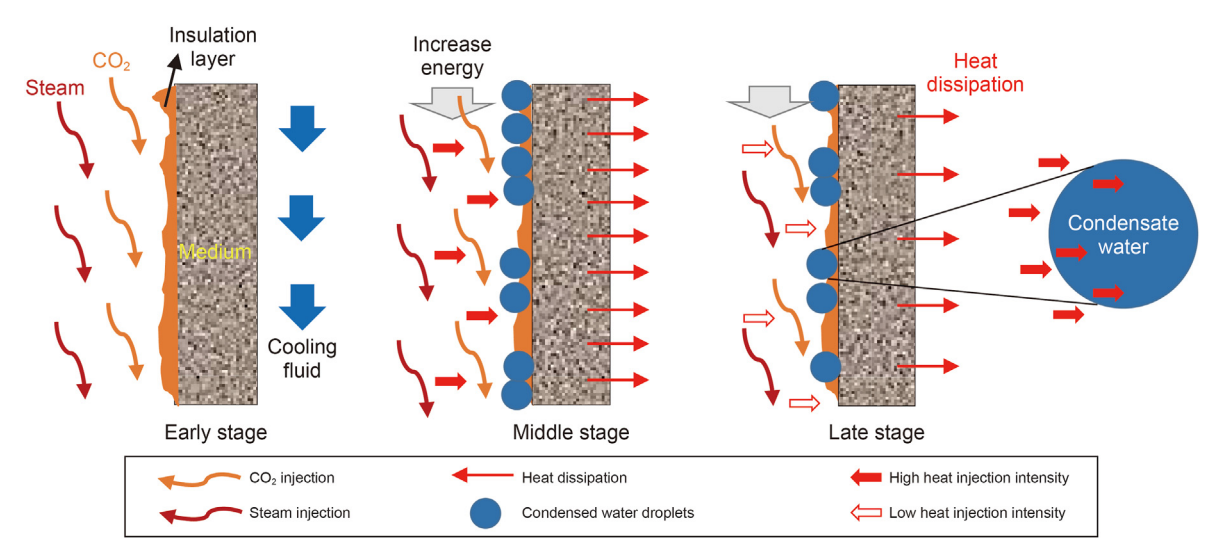


Fig. 10. Influence mechanism of CO<sub>2</sub> on the heat growth rate.

#### 3.2.1. Steam condensation and heat transfer

Steam injection rates of 5, 10, and 20 mL/min were applied to measure the temperature of the brass-based condenser block surface and the condensate water formation rate, as shown in Fig. 5.

As shown in Fig. 5, when the steam injection rate increased, the stable temperature of the steam heat transfer process gradually increased. In terms of condensation efficiency, when the steam injection rate was raised from 5 to 10 mL/min, the condensate water formation rate dramatically increased, reaching 61.9%. However, the condensate water formation rate dropped to 33.1% when the injection rate was raised to 20 mL/min. When the steam injection rate was slightly increased, viscous stress was generated on the gas-liquid interface between the steam and the condensed droplets. As the steam velocity was vertically downwards, the liquid film of the condensed droplets was thinned by the viscous stress. Thereby, the heat exchange was boosted, and the heat transfer process was accelerated. However, the steam flow accelerated to an uncontrollable level when the steam injection rate continued to increase. As a result, the steam was discharged without sufficient heat exchange, the heat transfer effect was poor, and the steam condensation was reduced.

The temperature of the cooling circulation system was set to 20, 40, and 60 °C to achieve different levels of undercooling. To compare the impacts of high-temperature channels at the back end of the steam drive and low-temperature channels at the front end of the steam drive on the steam flooding effect, the degree of undercooling was varied.

The statistical findings of the stable temperature and condensate water formation rate are presented in Fig. 6.

Fig. 6 illustrates that the condensation temperature difference increased as the undercooling increased. The surface heat transfer coefficient and the stable temperature of the condensing block surface increased.

When the steam injection rate was 5 mL/min, the stable temperature of the K-type thermocouples with different undercooling values was calculated, as shown in Fig. 7.

Fig. 7 shows that the temperature of the condensate block gradually increased with undercooling while maintaining the same injection rate. The figure also gives the fitting formula of the linear temperature distribution on the condensation block, where the slope represents the temperature gradient on the condensation block. The temperature gradient reflected the heat transfer intensity on the condensing surface (Kun and Kambiz, 2010). The temperature gradient changes for different steam injection rates and undercooling are shown in Fig. 8.

Note that with the same undercooling, the temperature gradient slightly increased with increasing steam injection rate. With the same steam injection rate, the temperature gradient significantly decreased as the undercooling increased. As a result, the steam heat transfer was more significantly influenced by the undercooling than by the steam injection rate.

The stable temperatures were 91.5, 89.8, and 84.9 °C when the degrees of undercooling were 60, 40, and 20 °C. Since the

**Table 3**Temperature and heat loss under different injection methods.

Injection method	Temperature of five thermocouples, °C			Heat loss, %		
	#1	#2	#3	#4	#5	
Steam	92.2	90.4	87.6	86.9	86.5	50.8
$Steam + CO_2$	88.8	86.0	85.6	84.5	82.6	48.9
$Steam + CO_2 + SDS$	81.1	80.4	80.0	79.1	78.6	47.9
$Steam + CO_2 + ZK\text{-}05200$	87.0	85.5	84.5	83.3	80.5	44.6

condensing block simulated the low-temperature porous medium, the stable temperature represented the heat loss caused by heat transfer between steam and low-temperature porous medium. Compared with the steam temperature at the inlet of the condensation chamber, the steam heat loss was 49.8% and 47.2% when the degrees of undercooling were 40 and 20 °C, respectively, whereas the heat loss reached 50.8% when the undercooling was 60 °C. The heat loss of steam was greater than 47% at any degree of undercooling, and the steam heat utilization rate was low. Therefore, it is critical to increase the heat dissipation resistance and to reduce the steam heat loss by adding CO2 and chemical agents.

### 3.2.2. Heat transfer of steam enhanced by $CO_2$ and adsorbed chemical

Existing studies have shown that the steam thermal effect was effectively improved and that the cost of heavy oil development was reduced by adding CO<sub>2</sub>. However, there is a paucity of detailed data describing the increase in steam heat utilization when CO<sub>2</sub> and chemicals are added (Dong et al., 2013; Andriianova and Leung, 2021; Zhang et al., 2020).

To clarify the mechanism of enhanced heat transfer, an experiment on the condensation heat transfer of  $CO_2$ —chemical assisted steam was developed. The experimental conditions were established as follows: steam injection temperature, 250 °C; steam injection rate, 5 mL/min; and undercooling, 20 °C. The influence of the  $CO_2$  injection rate on steam heat loss was experimentally investigated by changing the  $CO_2$  injection rate to 5, 10, and 20 mL/min. The experimental results are displayed in Fig. 9.

Due to the high condensation heat transfer coefficient, the heat transfer stable temperature was 92.2 °C during steam injection. With the addition of CO<sub>2</sub>, the condensation heat transfer coefficient decreased, and the stable temperature decreased to 88.7 °C. As shown in Fig. 11, the heat transfer stability time decreased (from point C to point A) when the CO<sub>2</sub> injection rate increased. This result was explained by the notion that as the CO<sub>2</sub> injection rate increased, the proportion of CO<sub>2</sub> in the mixed thermal fluid (CO<sub>2</sub> and steam) increased while the steam injection rate remained constant, which more easily inhibited the heat transfer of steam and reduced the steam heat loss along the path.

With the addition of CO<sub>2</sub>, the slope of the thermocouple average temperature curve (thermal growth rate) changed with time in a three-stage pattern, as shown in Fig. 9. The slope was small in the early stage, increased in the middle stage, and gradually stabilized in the late stage. Fig. 10 illustrates the process causing this behaviour.

In the early stage, the CO<sub>2</sub> initially made contact with the heat transfer medium due to the fast flow rate, forming an insulation layer. The subsequent condensation and heat dissipation of steam were prevented by the presence of an insulation layer and condensation water. During the middle stage, as the amount of steam injection increased, the condensation chamber was effectively pressurized, the steam flow velocity was enhanced, and the steam heat transfer efficiency was increased. Additionally, steam scour damaged part of the insulation layer, and the interface of the heat transfer medium was exposed, resulting in direct contact with the steam and facilitating heat exchange. In the later stage, the steam heat transfer efficiency decreased as the increase of the condensation surface heat.

To simulate chemical agent adsorption in the reservoir during oil extraction, SDS and betaine temperature-salt resistant foaming agents (ZK-05200) with a concentration of 0.5 wt% were applied on the surface of a brass-based condensing block. The experimental results of the stable temperature and condensate water formation rate under the combined influence of  $CO_2$  and chemical agents are shown in Fig. 11.

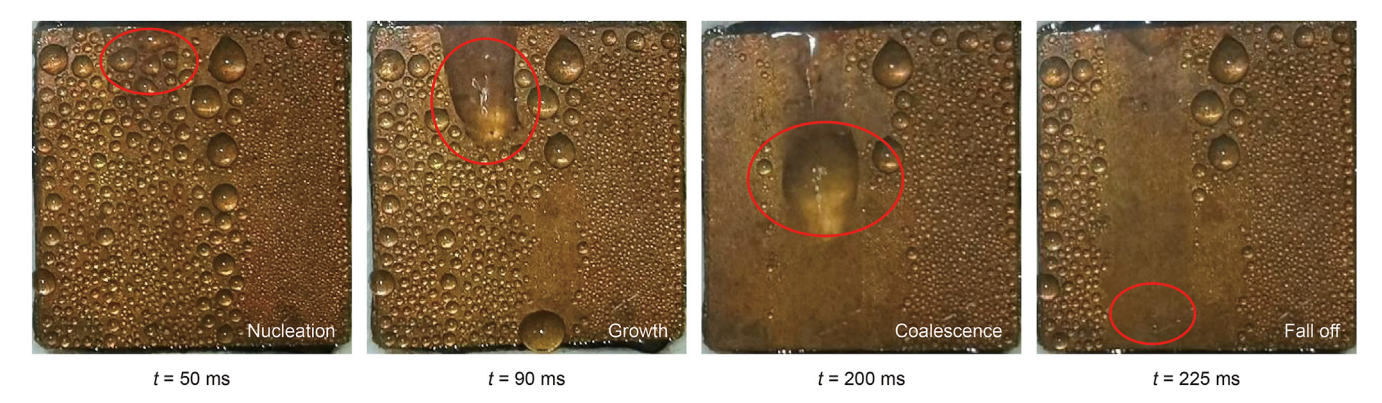


Fig. 12. The behaviour of one steam condensation cycle during steam injection.

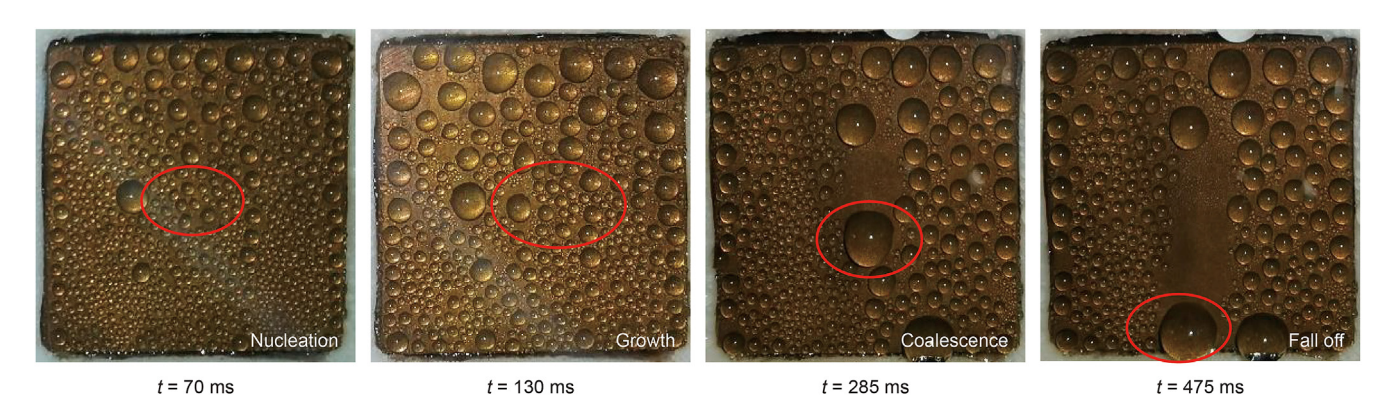


Fig. 13. The behaviour of one steam condensation cycle during  ${\rm CO_2}$ -assisted steam injection.

Fig. 11 demonstrates that the stable temperatures under the influence of steam— $CO_2$ —SDS and steam— $CO_2$ —ZK-05200 were 81.2 and 87.0 °C, respectively. It was proved that the heat transfer between steam and condensation surface was effectively hindered with the addition of  $CO_2$  and chemical agents, reducing the steam ineffective heat dissipation. Furthermore, compared with pure steam injection, the condensation heat transfer stability time was extended from 25 to 35 min during  $CO_2$  and chemical agents coinjection, increasing the steam heat transport distance.

After 25 min, the stable temperature of  $CO_2$ –ZK-05200 coinjection was comparable to that of  $CO_2$  single injection, indicating that the adhesion ability of SDS on the condenser block surface was stronger than that of ZK-05200. The ZK-05200 had been washed away at 25 min by the continual scouring of injected  $CO_2$  and steam, whereas SDS still hindered steam heat transfer at 35 min.

The temperature of the K-type thermocouples and the calculated heat loss (heat transport to condensation surface) for different injection methods are shown in Table 3. Compared with steam injection, heat loss was decreased by 1.9% with  $\rm CO_2$ —injection, 2.9% with  $\rm CO_2$ —ZK-05200 coinjection, and 6.2% with  $\rm CO_2$ —SDS coinjection, demonstrating that coinjecting  $\rm CO_2$  and SDS was the optimal combination for assisting steam flooding.

## 3.3. Micro mechanism of $CO_2$ and chemical agents affecting steam heat transfer

Steam condensation on the condensing block surface was divided into two primary modes: filmwise condensation and dropwise condensation (Gong et al., 2022). Filmwise condensation readily developed when the condensation liquid wetted the condensing block surface, and the condensate film enhanced the

heat transfer resistance. During dropwise condensation, when the size of the condensate liquid beads reached a critical diameter, gravity caused them to fall off. The fallen-off droplets swept other droplets along their path, and a constantly replenished condensation surface was provided (Bankoff and Mason, 2010).

Fig. 12 depicts a complete steam heat transfer and condensation cycle captured during steam injection.

Fig. 12 shows that in the steam injection process, the form of condensation heat transfer was conventional dropwise condensation.

Condensation and heat transfer were considered a complete cycle during droplet growth, merger, and fall-off. During steam injection, the droplets produced by steam condensation were evenly adsorbed on the surface of the condensation block and exhibited a modest size. The droplet quickly fell off, and a complete condensation cycle was maintained at approximately 200 ms. After the droplet fell off, the surface of the condensation block was in direct contact with the steam, and the condensation heat transfer coefficient increased.

The surface condensation behaviour of the condensate block observed during  $CO_2$ —assisted steam injection is depicted in Fig. 13. After adding  $CO_2$ , the condensation form maintained dropwise condensation, but the size of the condensation droplet notably increased. The addition of  $CO_2$  extended the condensation heat transfer cycle by 87.7%. As a noncondensate gas, the presence of  $CO_2$  reduced the partial pressure of the steam on the condensation surface, decreasing the saturation temperature of the steam, and lowering the driving temperature difference of heat transfer. The heat transfer of steam condensation was suppressed, and the condensate droplets fell off slowly. Coalescence and the remaining condensate droplets on the surface hindered the contact area

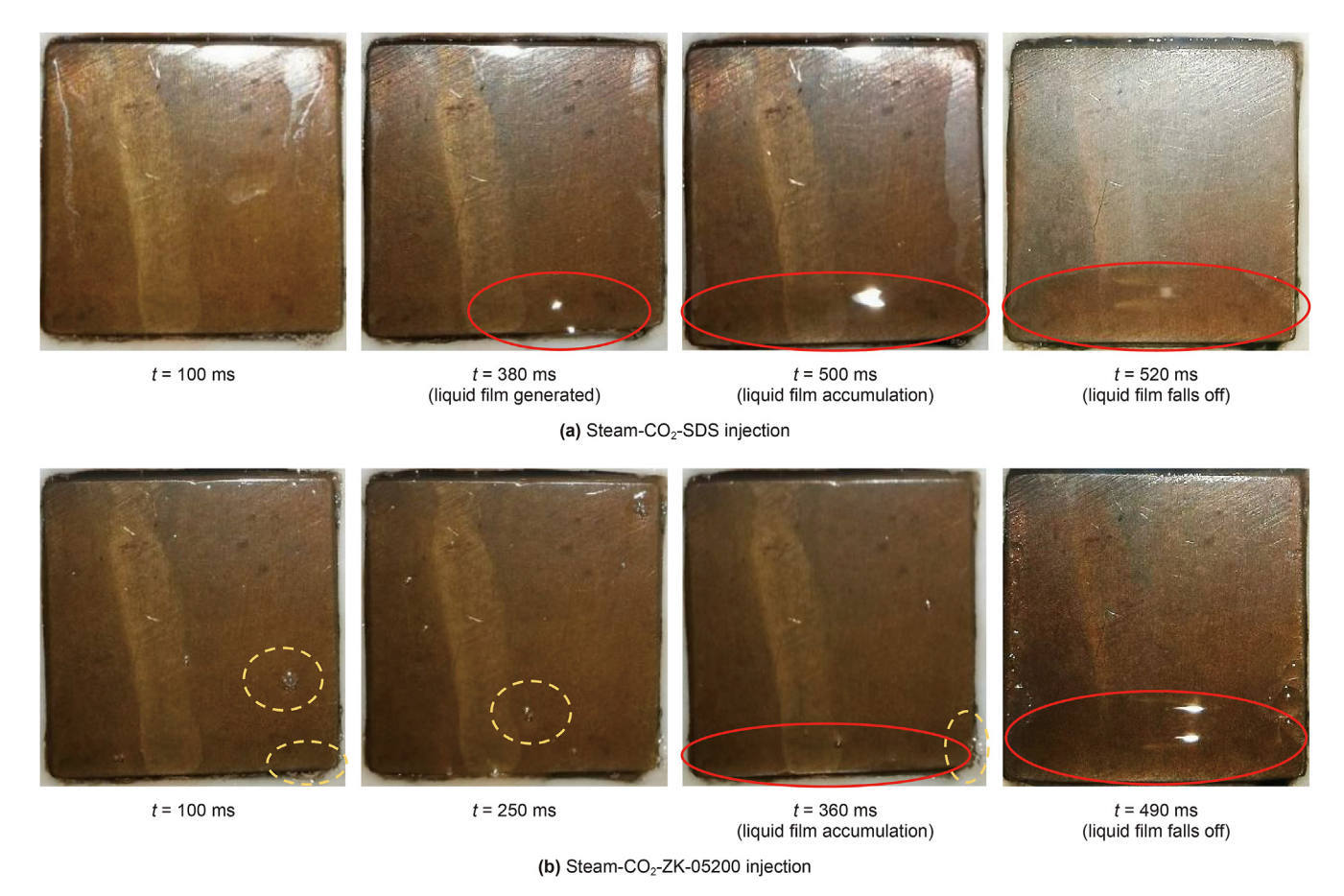


Fig. 14. Condensation behaviour of a condensation cycle during steam—CO<sub>2</sub>—chemical injection.

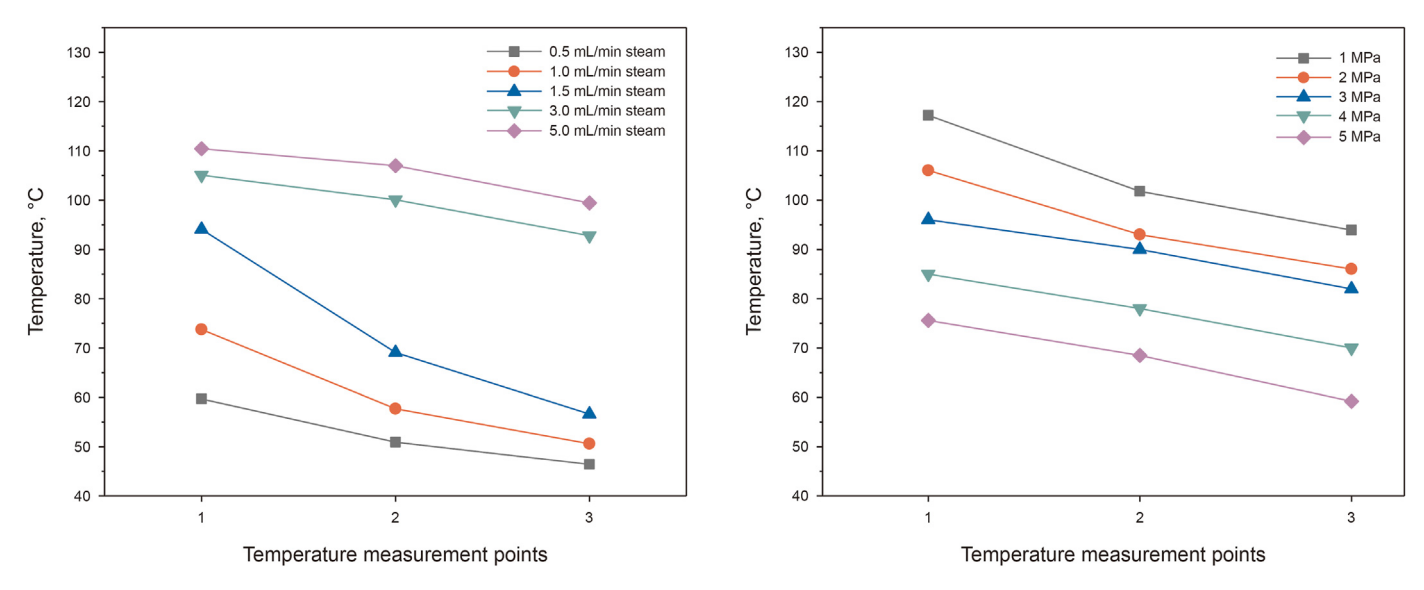


Fig. 15. Effect of steam injection rate on steam seepage heat transfer.

Fig. 16. Effect of injection pressure on stable temperature during steam seepage.

between the steam and the condensing block, reducing heat conduction.

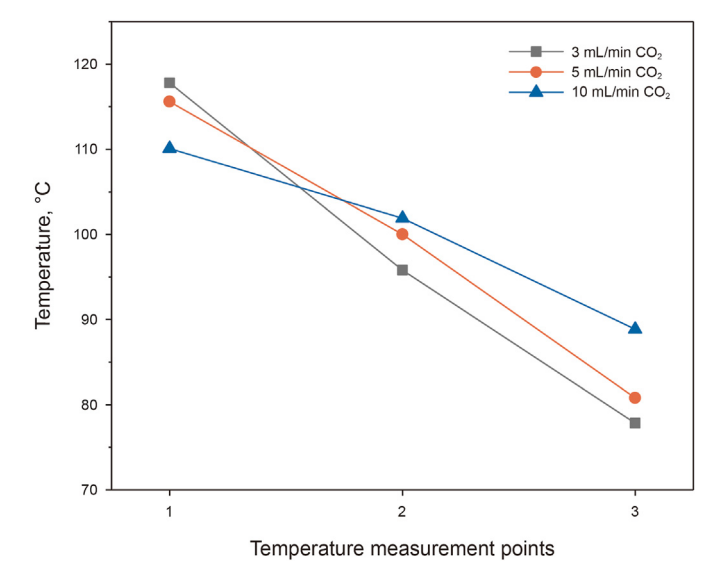
Under the synergistic action of  $CO_2$  and chemical agents, the complete cycle recorded from liquid film formation to falling off is exhibited in Fig. 14.

With the addition of SDS and a betaine temperature-salt

resistant foaming agent (ZK-05200), the surface of the brass-based condensation block displayed evident filmwise condensation. The heat transfer efficiency of dropwise condensation was ten to several times greater than that of filmwise condensation (Ma et al., 2001). When the condensation reached a specific threshold, the filmwise liquid film condensation slid off, and the subsequent condensation

**Table 4** Experimental parameters of steam seepage.

No.	Temperature of steam, °C	Experimental temperature, °C	Steam injection rate, mL/min	Injection pressure, MPa
1	250	65	0.5	0
2	250	65	1.0	0
3	250	65	1.5	0
4	250	65	3.0	0
5	250	65	5.0	0
6	250	65	1.5	1
7	250	65	1.5	2
8	250	65	1.5	3
9	250	65	1.5	4
10	250	65	1.5	5



 $\textbf{Fig. 17.} \ \ \text{Effect of CO}_2 \ \text{injection rate on stable temperature during steam seepage}.$ 

cycle started. Under the influence of  $CO_2$  and SDS, the condensation heat transfer coefficient was reduced by 31.6% on average, and the steam heat transfer cycle was extended by 1.3 times.

During ZK-05200 assisted steam injection, the condensation droplet formation and fall-off cycle was faster than that of SDS-assisted steam injection. The research in Section 3.2.2 demonstrated the synergistic effect of  $CO_2$  and SDS in increasing thermal resistance. Therefore, steam injection was subsequently assisted by the  $CO_2$  and SDS.

In addition, foam was produced at the interface of the condensation block after the ZK-05200 was added. Therefore, when applied in porous media, a chemical agent with foaming ability should be selected and injected with CO<sub>2</sub>. As a result of the chemicals and CO<sub>2</sub> being adsorbed on the porous media surface, foam may be generated following steam scouring, improving reservoir heterogeneity, blocking high permeability channels, and enhancing the recovery of steam flooding.

3.4. Enhancement of steam seepage by CO<sub>2</sub> and chemical agents

3.4.1. Effects of  ${\rm CO_2}$  and chemical injection parameters on steam heat conduction

To explore the heat transfer of steam seepage under the impact of different injection settings, the steam injection rate and pressure were adjusted in the steam—CO<sub>2</sub>—chemical seepage experiment, as illustrated in Figs. 15 and 16.

The experimental parameters are shown in Table 4.

Observing the temperature under different steam injection rates, when the steam injection flow rate was 1–1.5 mL/min, the temperature at measurement point 1 noticeably increased. In contrast, the increase in temperature at measurement point 3 was minimal, indicating that the propagation of steam heat was low. When the steam injection rate was 3 mL/min, the steam thermal sweep range covered the whole sandpack model, and the temperature variation throughout the model was minimal. The overall temperature of the sandpack slightly increased as the steam injection rate continued to rise.

When the steam flowed in the sandpack, with heat being transferred to the surrounding porous medium, the sandpack temperature increased, and the steam temperature decreased. The strength of heat injection was low when the steam injection rate was small, the steam flow rate was sluggish, and the amount of heat injected per unit time was tiny. As a result, the heat carried by the steam was swiftly discharged during steam seepage and could not be transferred to the back end of the sandpack model. As the steam injection rate increased, the strength of the heat injection increased, and the steam seepage velocity increased. The back end of the sandpack model received additional heat through steam, and the thermal sweep range widened.

Since the properties of steam and  $CO_2$  were influenced by pressure, the effect of injection pressure on steam seepage heat transfer was investigated by maintaining the steam injection rate constant at 1.5 mL/min and by varying the steam injection pressure to 1, 2, 3, 4, and 5 MPa.

As the steam injection pressure increased, the temperature of the sandpack decreased. The temperatures of the three measurement points were 127.2, 111.8, and 103.9 °C, respectively, at 1 MPa steam injection pressure. When the steam injection pressure was

**Table 5** Experimental parameters of CO<sub>2</sub>—chemical assisted steam seepage.

No.	Steam injection rate, mL/min	Injection pressure, MPa	CO <sub>2</sub> injection rate, mL/min	Injection amount of chemical agent, PV	Type of chemical agent
1	1.5	1	3	0.1	SDS
2	1.5	1	5	0.1	SDS
3	1.5	1	10	0.1	SDS
4	1.5	1	5	0.2	SDS
5	1.5	1	5	0.3	SDS
6	1.5	1	5	0.3	ZK-05200 (foaming agent)

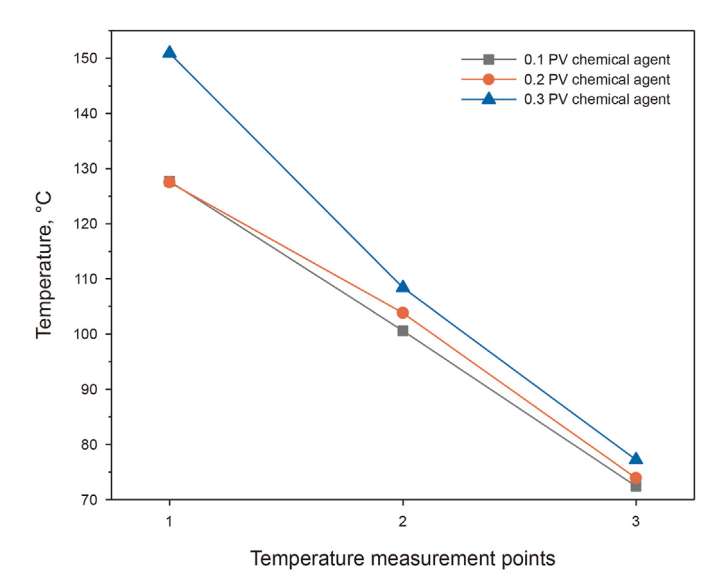


**Fig. 18.** Effect of chemical injection volume on stable temperature during steam seepage.

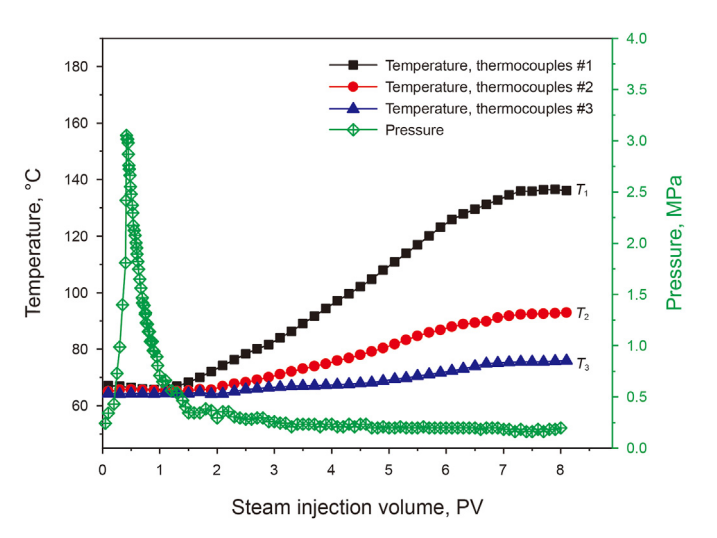


Fig. 19. Variations of temperature and pressure during seepage of pure steam.

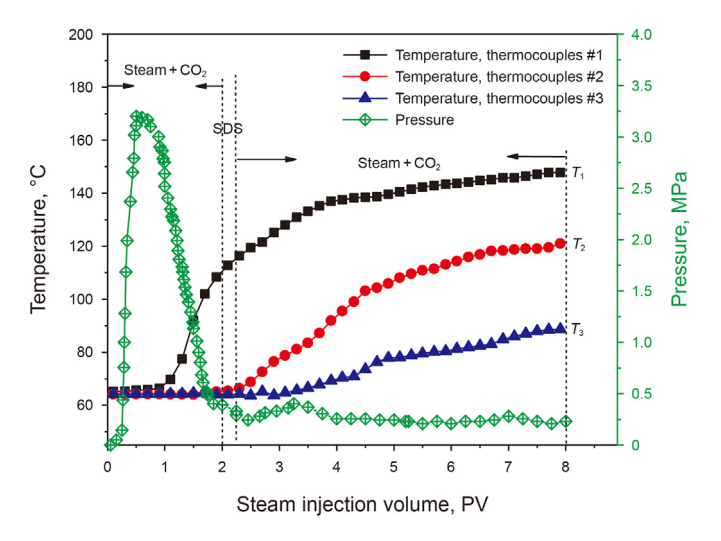


Fig. 20. Variations of temperature and pressure during seepage of  ${\rm CO_2-SDS}$  assisted steam.

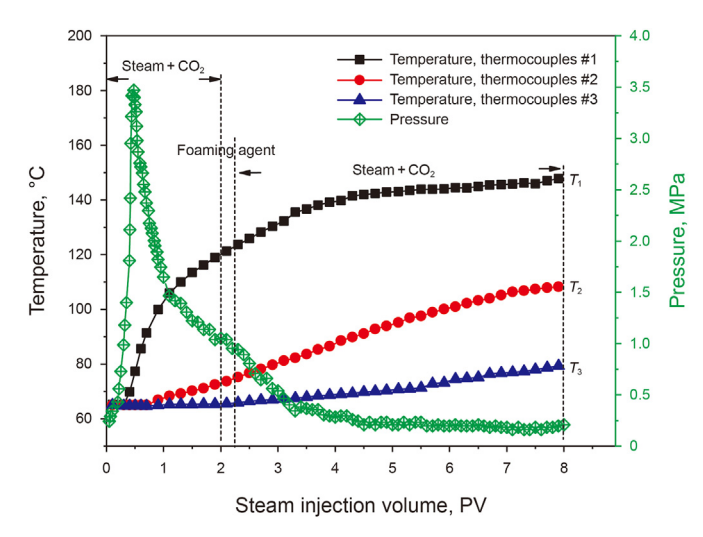


Fig. 21. Variations of temperature and pressure during seepage of CO<sub>2</sub>—foaming agent assisted steam.

5 MPa, the temperature of the three measurement points decreased to 85.6, 78.5, and 69.2  $^{\circ}$ C.

This phenomenon occurred as the saturation temperature needed to maintain the steam state was increased when the steam injection pressure increased, and the steam more easily condensed into hot water. Both the heat capacity and transported heat diminished after the steam condensed into hot water. Therefore, it was necessary to reduce the steam injection pressure to make the steam transfer heat to the deep formation, which also reflected the importance of reducing the formation pressure for steam flooding.

The influence of different CO<sub>2</sub> injection rates on steam heat conduction is summarized in Fig. 17. The experimental settings for the steam seepage are displayed in Table 5.

As the  $CO_2$  injection rate increased, the  $CO_2$  injection amount increased. Notably, the temperature at measurement points 2 and 3 increased by  $2.96-11.03\,^{\circ}C$  with an increase in the  $CO_2$  injection. This phenomenon depicted that as the  $CO_2$  injection rate increased, the injection rate of  $CO_2$ —steam mixed fluid increased, causing the temperature of the back end of the model to rise at a faster rate. On the other hand, the quantity of  $CO_2$  in the mixed fluid increased, which was beneficial to inhibiting steam heat transfer at the front end of the model, allowing more heat to be transferred to the back end of the model.

The steam injection rate was maintained at 1.5 mL/min in the steam seepage experiment. The quantity of chemical agents was changed to examine the impact of various surfactant ratios on steam heat conduction, as shown in Fig. 18.

According to Fig. 18, the volume of chemical injection significantly influenced the steam heat conduction. Since the chemical was injected at room temperature, the greater the injection volume is, the longer the cooling process, and the slower the subsequent temperature rise. When the volume of the chemical agent injected was increased to 0.3 PV, the temperature of the model significantly increased, and the temperature of the three measurement points increased by 23.2, 7.8, and 4.8 °C. When the injection volume of the chemical agent was large, the channel was blocked, and the CO<sub>2</sub> steam was difficult to break through, which produced the large temperature rise at the front end of the model. The steam was gathered at measurement point 1, and the temperature at the front end of the model increased.

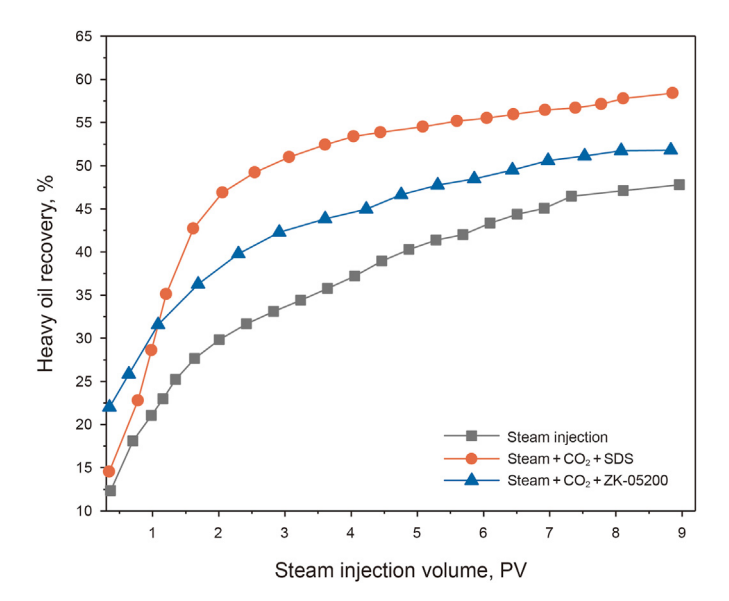


Fig. 22. Heavy oil recovery of different injection methods.

### 3.4.2. CO<sub>2</sub>—chemical assisted steam to increase steam stable temperature and oil recovery

According to Fig. 15, when the steam injection rate was 1.5 mL/min, there was a considerable temperature change with the sand-pack model, making it easy to compare the effect of adding CO<sub>2</sub> and SDS. The smaller injection pressure was better to help the steam heat transformed to the back end of the sandpack model. Therefore, in the steam—CO<sub>2</sub>—chemical seepage experiment, the sandpack model was located in a thermostat with an ambient temperature of 65 °C. The steam injection temperature was set to 250 °C, the steam injection rate was 1.5 mL/min, and the injection pressure was 0.1 MPa. Figs. 19—21 illustrate the analysis of the temperature and pressure variations in the sandpack model with chemical agents.

Fig. 19 indicates that the temperatures at measurement points 1 to 3 were 136.1, 92.9, and 75.9 °C during steam injection. The temperature significantly dropped along the seepage process, causing to a large heat loss.

The temperature distribution was improved, and the heat sweep range was expanded when steam seepage was assisted by chemical agents and CO<sub>2</sub>. The temperatures at measuement points 1, 2 and 3 were increased to 147.8, 108.2, and 79.4 °C with the injection of CO<sub>2</sub>-ZK-05200, and were increased to 150.7, 121, and 88.7 °C with the injection of CO<sub>2</sub>-SDS. The heat transfer from the steam to porous media decreased with the injection of CO<sub>2</sub>-SDS, and more steam heat was transferred to the back end of the sandpack model. CO<sub>2</sub> easily flowed in porous media because of the low seepage resistance. When steam and CO<sub>2</sub> were combined, the steam seepage was enhanced by CO<sub>2</sub>, and the contact time between the steam and the porous media was shortened, making steam quickly penetrate the back end of the sandpack, and reducing the heat loss. On the other hand, CO2 and SDS created a "film" on the surface of low-temperature porous media. Under the action of the "film", the heat transfer resistance increased, and the heat transfer was blocked.

The heavy oil recovery of different injection methods is shown in Fig. 22.

As shown in Fig. 22, the heavy oil recovery during steam injection, steam— $CO_2$ —SDS injection, and steam— $CO_2$ —foaming agent injection were 48.19%, 58.01%, and 51.8%, respectively. Steam— $CO_2$ —SDS coinjection had the best effect on oil displacement and viscosity reduction.

By comparing the pressure curves in Figs. 19–21, the maximum pressure of the sandpack model during steam— $CO_2$ —foaming agent injection was 3.47 MPa. Thus, the coinjection of  $CO_2$ —foaming agent was superior for supplementing the formation energy. During  $CO_2$ —SDS coinjection, the pressure of the sandpack model reached 3.2 MPa, and the formation energy was boosted. SDS served numerous purposes as an organic solvent, such as dissolving in heavy oil to reduce viscosity and altering reservoir wettability. Compared with pure steam injection, the heavy oil recovery improved by 9.82% under the steam— $CO_2$ —SDS coinjection.

#### 4. Conclusions

- (1) The steam condensation heat transfer coefficient increased with the steam injection rate and undercooling and decreased with the CO<sub>2</sub> injection rate. The condensation form changed to filmwise condensation during the CO<sub>2</sub>—chemical assisted steam injection. The condensation heat transfer coefficient was reduced by 31.6% on average, and the steam heat transfer cycle was lengthened by 1.3 times in the process of steam—CO<sub>2</sub>—chemical injection.
- (2) The temperature at the back end of the sandpack model significantly increased by 3.5–12.8 °C by adding CO<sub>2</sub> and chemical agents. CO<sub>2</sub> opened up the seepage channels for steam, making steam enter the back end of the sandpack model at a faster rate. On the other hand, the "film" created by the CO<sub>2</sub> and chemical agent restricted the heat transfer of the steam at the sandpack inlet, causing more steam heat to be carried to the back end of the sandpack model.
- (3) The CO<sub>2</sub>—SDS coinjection significantly enhanced steam flooding. First, with the injection of CO<sub>2</sub>, the steam saturation temperature decreased, and the heat dissipation of steam was hindered. Second, CO<sub>2</sub> improved the steam heat transfer range. Third, the heavy oil viscosity was reduced by emulsification of the CO<sub>2</sub>—chemical emulsion. Therefore, the heavy oil recovery was improved by 9.82% and the steam heat loss was reduced to 6.2%.
- (4) According to the experimental results of steam seepage, some suggestions were made for field application. As the steam injection rate increased, the steam sweep range increased. The smaller injection pressure was better to help the steam heat transformed to the back end of the sandpack model. Moreover, the CO<sub>2</sub> and chemical agent coinjection can considerably increase the temperature in the back end of sandpack model.

#### **Declaration of competing interest**

The authors declared that there is no conflict of interest.

#### Acknowledgements

The authors appreciate the financial support of the National Nature Science Foundation of China (Grant No. U20B6003) and the Natural Science Foundation of Shandong Province, China (ZR2020QE106).

#### References

Ahmadi, M., Chen, Z., 2020. Challenges and future of chemical assisted heavy oil recovery processes. Adv. Colloid. Interfac. 275, 1–27. https://doi.org/10.1016/icis.2019.102081

Aklilu, Y.A., Cho, S., Zhang, Q., Taylor, E., 2018. Source apportionment of volatile organic compounds measured near a cold heavy oil production area. Atmos. Res. 206, 75–86. https://doi.org/10.1016/j.atmosres.2018.02.007.

Alvarado, V., Manrique, E., 2010. Enhanced oil recovery: an update review. Energies

- 3 (9), 1529-1575. https://doi.org/10.3390/en3091529.
- Andriianova, E., Leung, J.Y., 2021. A statistical upscaling workflow for warm solvent injection processes for heterogeneous heavy oil reservoirs. Nat. Resour. Res. 1–21. https://doi.org/10.1007/s11053-021-09921-6.
- Azad, M.S., Trivedi, J.J., 2019. Quantification of the viscoelastic effects during polymer flooding: a critical review. SPE J. 24 (6), 1–27. https://doi.org/10.2118/195687-PA.
- Balaji, C., Srinivasan, B., Gedupudi, S., 2021. One-dimensional, steady state heat conduction. Heat Tran. Eng. 15–64. https://doi.org/10.1016/B978-0-12-818503-2.00002-2.
- Bankoff, S.G., Mason, J.P., 2010. Heat transfer from the surface of a steam bubble in turbulent subcooled liquid stream. AIChE J. 8 (1), 30–33. https://doi.org/10.1002/aic.690080110.
- Brame, S.D., Li, L., Mukherjee, B., Patil, P.D., Potisek, S., Nguyen, Q.P., 2019. Organic bases as additives for steam-assisted gravity drainage. Petrol. Sci. 6, 1332–1343. https://doi.org/10.1007/s12182-019-0341-7.
- Canbolat, S., Kut, D., Dayioglu, H., 2013. Investigation of pumice stone powder coating of multilayer surfaces in relation to acoustic and thermal insulation. J. Ind. Textil. 44 (4), 639–661. https://doi.org/10.1177/1528083713516665.
- Dong, X., Liu, H., Chen, Z., 2021. Existing problems for steam-based enhanced oil recovery processes in heavy oil reservoirs. Dev. Petrol. Sci. 73, 47–98. https:// doi.org/10.1016/B978-0-12-823954-4.00005-9.
- Dong, Z.X., Li, Y., Lin, M.Q., 2013. A study of the mechanism of enhancing oil recovery using supercritical carbon dioxide micro emulsions. Petrol. Sci. 10, 91–96. https://doi.org/10.1007/s12182-013-0254-9.
- 91–96. https://doi.org/10.1007/s12182-013-0254-9.
  Gong, L., Zhao, D., Guo, Y., Chen, K., Shen, S., 2022. The coupling process of steam condensation and falling film evaporation with non-condensable gas. Int. J. Therm. Sci. 172. 107201. https://doi.org/10.1016/j.iithermalsci.2021.107201.
- Guo, K., Li, H., Yu, Z., 2016. In-situ heavy and extra-heavy oil recovery: a review. Fuel 185, 886–902. https://doi.org/10.1016/j.fuel.2016.08.047.
- Hasan, A.R., Kabir, C.S., Lin, D., 2005. Analytic wellbore-temperature model for transient gas-well testing. SPE Reservoir Eval. Eng. 8, 240–247. https://doi.org/ 10.2523/84288-MS.
- Hou, Q.D., Ju, M.T., Li, W.Z., Liu, L., Yang, Q., 2017. Pretreatment of lignocellulosic biomass with ionic liquids and ionic liquid-based solvent systems. Molecules 22 (3), 490–498. https://doi.org/10.3390/molecules22030490.
- Kun, Y., Kambiz, V., 2010. Analysis of temperature gradient bifurcation in porous media-An exact solution. Int. J. Heat Mass Tran. 53 (19–20), 4316–4325. https://doi.org/10.1016/j.ijheatmasstransfer.2010.05.060.
- Law, D.H.S., 2004. Disposal of carbon dioxide, a greenhouse gas, for pressure maintenance in a steam-based thermal process for recovery of heavy oil and bitumen. SPE International Thermal Operations and Heavy Oil Symposium and Western Regional Meeting. https://doi.org/10.2118/86958-MS.
- Li, B., Zhang, Q., Li, S., Li, Z., 2017. Enhanced heavy oil recovery via surfactant-assisted CO<sub>2</sub> huff-n-puff process. J. Petrol. Sci. Eng. 159, 25–34. https://doi.org/10.1016/j.petrol.2017.09.029.
- Li, M., 2012. Coupled thermo-hydro analysis of steam flow in a horizontal wellbore in a heavy oil reservoir. Petrol. Sci. 9, 298–305. https://doi.org/10.1007/S12182-012-0234-5.
- Li, S.Y., Han, R., Wang, P., Cao, Z.J., Li, Z.M., Ren, G.W., 2022a. Experimental investigation of innovative superheated vapor extraction technique in heavy oil reservoirs: a two-dimensional visual analysis. Energy 238, 121882. https://doi.org/10.1016/j.energy.2021.121882.
- Li, S.Y., Sun, L., Wang, L., Li, Z.M., Zhang, K.Q., 2022b. Hybrid CO<sub>2</sub>–N<sub>2</sub> huff-n-puff strategy in unlocking tight oil reservoirs. Fuel 309, 122198. https://doi.org/

#### 10.1016/j.fuel.2021.122198.

- Liu, H., Cheng, L., Xiong, H., Huang, S., 2017. Effects of solvent properties and injection strategies on solvent-enhanced steam flooding for thin heavy oil reservoirs with semi-analytical approach. Oil Gas Sci. Technol. 72 (4), 1–15. https://doi.org/10.2516/ogst/2017015.
- Ma, Q., Li, H., Li, Y., 2020. The study to improve oil recovery through the clay state change during low salinity water flooding in sandstones. ACS Omega 5 (46), 29816–29829. https://doi.org/10.1021/acsomega.0c03849.
- Ma, X.H., Tao, B., Chen, J.B., Xu, D.Q., Lin, J.F., 2001. Dropwise condensation heat transfer of steam on a polytethefluoroethylene film. J. Therm. Sci. 10 (3), 247–253. https://doi.org/10.1007/s11630-001-0027-4.
- Mukherjee, B., Patil, D.P., Gao, M., Miao, W., Rozowski, P., 2018. Laboratory evaluation of novel surfactant for foam assisted steam EOR method to improve conformance control for field applications. SPE. Improv. Oil. Recov. Conf. https://doi.org/10.2118/190263-MS.
- Pang, Z., Qi, P., Zhang, F., Ge, T., Liu, H., 2018. The experimental analysis about the role of flue gas injection for horizontal well steam flooding. J. Energ. Resour-Asme. 140 (10), 102902–102913. https://doi.org/10.1115/1.4039870.
- Sharma, J., Gates, I.D., 2010. Multiphase flow at the edge of a steam chamber. Can. J. Chem. Eng. 88 (3), 312–321. https://doi.org/10.1002/cjce.20280.
- Shi, L., Ye, Z., Zhang, Z., Zhou, C., Zhu, S., Guo, Z., 2010. Necessity and feasibility of improving the residual resistance factor of polymer flooding in heavy oil reservoirs. Petrol. Sci. 7, 251–256. https://doi.org/10.1007/s12182-010-0029-5.
- Tian, Z., Gan, W.L., Qi, Z.X., Tian, M.L., Gao, W.Z., 2022. Experimental study of organic Rankine cycle with three-fluid recuperator for cryogenic cold energy recovery. Energy 242. https://doi.org/10.1016/j.energy.2021.122550.
- Wan, T., Wang, X.J., Jing, Z.Y., Gao, Y., 2020. Gas injection assisted steam huff-n-puff process for oil recovery from deep heavy oil reservoirs with low-permeability. I. Petrol. Sci. Eng. 185. 1–16. https://doi.org/10.1016/j.petrol.2019.106613.
- j. Petrol. Sci. Eng. 185, 1–16. https://doi.org/10.1016/j.petrol.2019.106613.

  Wang, J.L., Feng, J.X., Bentley, Y., Feng, L.Y., 2017. A review of physical supply and EROI of fossil fuels in China. Petrol. Sci. 14, 806–821. https://doi.org/10.1007/s12182-017-0187-9
- Wang, Z.J., Li, S.Y., Li, Z.M., 2022. A novel strategy to reduce carbon emissions of heavy oil thermal recovery: condensation heat transfer performance of flue gas-assisted steam flooding. Appl. Therm. Eng. 205, 1–13. https://doi.org/10.1016/j.applthermaleng.2022.118076.
- Wang, H.T., Zeng, M.L., Lv, C.Y., Lang, D.J., Luo, M., Zhao, Q.M., Zhao, C.P., 2020. Nuclear-magnetic-resonance study on oil mobilization in shale exposed to CO<sub>2</sub>. SPE J. 25 (1), 432–439. https://doi.org/10.2118/190185-PA.
- Wang, Z.Z., Li, Z.M., Sarma, H.K., Xu, Y.J., Wu, P., Yang, J.P., Wang, H.Y., Lu, T., 2019. A visualization experimental study on gas penetration through interlayer to improve SAGD performance. J. Petrol. Sci. Eng. 7, 959–970. https://doi.org/ 10.1016/j.petrol.2019.03.001.
- Wu, Z.B., Liu, H.Q., Wang, X., 2018. Adaptability research of thermal-chemical assisted steam injection in heavy oil reservoirs. J. Energ. Resour-Asme. 140 (5). https://doi.org/10.1115/1.4038405, 052901.1-052901.7.
- Xu, Z.X., Li, S.Y., Li, B.F., Chen, D.Q., Liu, Z.Y., Li, Z.M., 2020. A review of development methods and EOR technologies for carbonate reservoirs. Petrol. Sci. 17, 990–1013. https://doi.org/10.1007/s12182-020-00467-5.
- Zare, A., Hamouda, A.A., 2019. Coinjection of C<sub>6</sub>, C<sub>7</sub>, and CO<sub>2</sub> with steam to improve low-pressure SAGD process. Fuel 238, 394–401. https://doi.org/10.1016/j.fuel.2018.10.100.
- Zhang, C., Xi, L.H., Wu, P.K., Li, Z.M., 2020. A novel system for reducing CO<sub>2</sub>—crude oil minimum miscibility pressure with CO<sub>2</sub>—soluble surfactants. Fuel 281, 118690. https://doi.org/10.1016/j.fuel.2020.118690.